Computational Strategies for Modeling Distributed Random Excitations (Diffuse Field and Turbulent Boundary Layer) in a Vibro-Acoustic Context

J.-P. Coyette, B. Van Den Nieuwenhof, G. Lielens et Y. Detandt
Free Field Technologies S.A, Rue Emile Francqui, 9, 1435 Mont Saint Guibert, Belgique
jean-pierre.coyette@fft.be

The paper reviews some key ingredients of an efficient computational strategy for handling distributed random excitations (diffuse field or turbulent boundary layer) in a vibro-acoustic context. Considered random excitations are described as homogeneous weakly stationary random processes and are therefore described by auto-power spectra and spatial correlation functions. A particular attention is devoted to the elimination of grazing incidences for diffuse fields and to the selection of appropriate semi-empirical models for TBL excitations. Mesh requirements related to an algebraic sampling strategy of such excitations are highlighted, with a particular emphasis on the effect of the convective flow velocity. The evaluation of the random response is addressed both in direct and modal contexts. Academic and industrial applications are presented. Comparison with reference analytical solutions are also provided.

1 Introduction

Random excitations (diffuse field, turbulent boundary layer) are frequently encountered in vibro-acoustic applications. The distributed nature of such excitations requires some attention in a discrete finite element context and is further examined in this contribution. Specific aspects related to diffuse filed and TBL excitations are described in the first two sections while efficient computational strategies are presented and illustrated in the last two sections.

2 Diffuse field

2.1 Introduction

The 'diffuse field' concept is important in many acoustic applications since it is directly related to the sound field in a reverberant chamber traditionally involved in experimental or numerical acoustic transmission studies. The characterization of a diffuse field can be found in many references ([1] and [2], for example). The purpose of this section is the examination of a limitation of incidence angles in the treatment of an acoustic diffuse field. The elimination of grazing incidences can be investigated in two particular contexts. The first one refers to the the modeling of a diffuse field as a weakly stationary random process while the second one refers to a more direct approximation of a diffuse field using a sampling procedure (modeling the diffuse field as a sum of discrete plane waves).

2.2 Diffuse field related to an infinite set of plane waves

A perfect diffuse field can be obtained by summing up the effect of an infinite number of uncorrelated plane waves whose directions are equally spatially spread. The present derivation is based on [3] and starts with the expression of the pressure field related to a particular plane wave (index n). This field can be expressed as $p_n(\mathbf{r}, t)$ where $\mathbf{r} = (r, \theta, \phi)$ is the vector position (in spherical coordinates) of the considered evaluation point (see Figure 1) and t is the time.

Since the objective is the evaluation of the spatial correlation function, two particular points are considered along axis 1 : the first point (labeled ξ_1) is located at the origin while the second point (labeled ξ_2) is located at coordinates $(r, 0, 0)$.
If one denotes by $x_n(t)$ the instantaneous pressure value at the origin for the considered plane wave :

$$x_n(t) = p_n(0, t) \, , \tag{1}$$

one can easily retrieve the pressure at location r along axis 1 by converting the spatial interval into an equivalent time

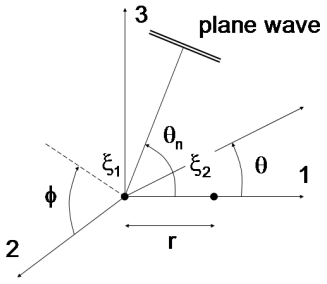

Figure 1 – Coordinate system and particular plane wave.

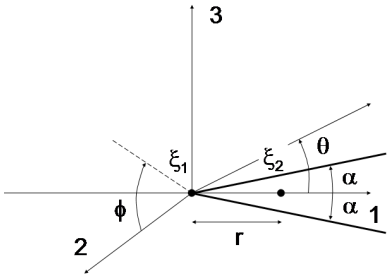

Figure 2 – Limitation of grazing incidences.

interval [3] :

$$p_n(r, t) = p_n\left(0, t - \frac{r}{c}\cos\theta_n\right) = x_n\left(t - \frac{r}{c}\cos\theta_n\right) \, . \tag{2}$$

2.3 Derivation of the spatial correlation function with elimination of grazing incidences

The usual correlation function of a diffuse field can be expressed as :

$$R(r, \tau) = \frac{1}{4\pi}\int_{-\pi/2}^{+\pi/2}\int_{0}^{2\pi} R_0\left(\tau - \frac{r}{c}\cos\theta\right)|\sin\theta| \, d\phi d\theta \, . \tag{3}$$

where $R_0(\tau)$ is the auto-correlation function of $x_n(t)$ signals.

If the objective is to eliminate grazing incidences, one can introduce a restriction concerning plane wave incidence angles. With reference to Figure 2, this leads to incidence angles θ given by :

$$-\frac{\pi}{2} \le \theta \le -\alpha \;\text{ or }\; \alpha \le \theta \le \frac{\pi}{2} \, . \tag{4}$$

Equation (3) can therefore be rewritten in the following

form :

$$R(r,\tau) = \frac{1}{4\pi}\left(\int_{-\pi/2}^{-\alpha}\int_{0}^{2\pi} R_0\left(\tau - \frac{r}{c}\cos\theta\right)|\sin\theta|\, d\phi d\theta + \int_{\alpha}^{\pi/2}\int_{0}^{2\pi} R_0\left(\tau - \frac{r}{c}\cos\theta\right)\sin\theta d\phi d\theta\right) . \quad (5)$$

Since the first integral is equal to the second one, the following expression is easily obtained after integration along ϕ :

$$R(r,\tau) = \int_{\alpha}^{\pi/2} R_0\left(\tau - \frac{r}{c}\cos\theta\right)\sin\theta d\theta . \quad (6)$$

By the same change of variable :

$$t = \tau - \frac{r}{c}\cos\theta , \quad (7)$$

this equation can be rewritten as :

$$R(r,\tau) = \frac{c}{r}\int_{\tau-\frac{r}{c}\cos\alpha}^{\tau} R_0(t)\, dt . \quad (8)$$

This expression can be formulated in terms of the power spectral density $S_0(\omega)$:

$$R(r,\tau) = \frac{c}{r}\int_{\tau-\frac{r}{c}\cos\alpha}^{\tau} R_0(t)\, dt , \quad (9)$$

$$= \frac{c}{r}\int_{\tau-\frac{r}{c}\cos\alpha}^{\tau}\int_{-\infty}^{+\infty} S_0(\omega)\, e^{i\omega t} d\omega dt , \quad (10)$$

$$= \frac{c}{r}\int_{-\infty}^{+\infty} S_0(\omega)\left[e^{i\omega t}\right]_{\tau-\frac{r}{c}\cos\alpha}^{\tau} d\omega , \quad (11)$$

$$= \frac{c}{\omega r}\int_{-\infty}^{+\infty} S_0(\omega)\sin\left(\frac{\omega r\cos\alpha}{c}\right)e^{i\omega\tau} d\omega . \quad (12)$$

so that the spatial correlation function f_c is given by

$$f_c(r,\omega) = \frac{c}{\omega r}\sin\left(\frac{\omega r\cos\alpha}{c}\right) = \frac{\sin(kr\cos\alpha)}{kr} . \quad (13)$$

2.4 Examination of the correlation function

For practical purpose, it is more convenient to define alternatively the restriction about incidence angles and to scale the correlation function so that it is equal to 1 for $r = 0$. Instead of referring to angle θ defined with reference to axis 1 (Figure 2) :

$$-\frac{\pi}{2} \le \theta \le -\alpha \quad \text{or} \quad \alpha \le \theta \le \frac{\pi}{2} , \quad (14)$$

one can introduce a normal incidence angle θ' (Figure 3) :

$$\theta' \le \beta . \quad (15)$$

Further division by $\sin\beta$ leads to the final form of the updated correlation function :

$$f_c(r,\omega) = \frac{\sin(kr\sin\beta)}{kr\sin\beta} . \quad (16)$$

This operation can be interpreted as a scaling of the excitation in order to keep the same mean quadratic pressure along the loaded surface for any β value. The effect of a limitation of incidence angles is examined by a comparison of the spatial correlation function (Figure 4) for the following values of β angle : 60, 70 and 80 degrees. The related spatial correlation functions are compared to the conventional form (corresponding to $\beta = 90$ degrees) which do not eliminate grazing incidences. As expected, a reduction of the maximum incidence angle β leads to a more correlated excitation.

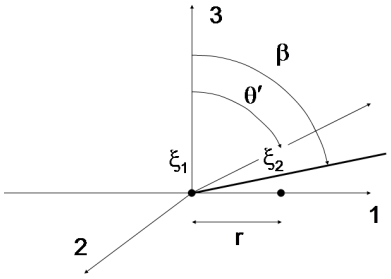

FIGURE 3 – Normal incidence angles.

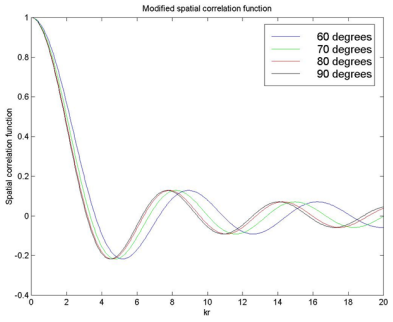

FIGURE 4 – Comparison of spatial correlation function for various maximum normal incidence angles.

2.5 Sampling a diffuse field with elimination of grazing incidences

The sampling procedure relies on the definition of a finite set of plane waves with random phases. The main issue is to achieve an equi-repartition of these plane waves along a spherical (or hemi-spherical) surface with a possible elimination of grazing incidences. In this context, the β angle can be selected in order to define the acoustic volume supporting the generation of plane waves. The discrete incidence angles depend on the specification of the β value and the number of parallel sectors N. Further information can be found in [4].

3 Turbulent boundary layer excitation

3.1 Introduction

As for diffuse field excitations, the numerical treatment of a TBL excitation can rely on different computational strategies. A common point of all strategies is the need to resolve the distributed random excitation along a discrete surface. Usually the mesh resolution is fixed by the dynamic behavior of the mechanical structure. The main purpose of this section is to highlight the capacity of the mesh to resolve spatial correlation effects along the loaded surface. This is done by examining the spatial correlation function related to Corcos model and evaluating the element contributions to the mean quadratic incident pressure (or, equivalently, to the incident power). Numerical simulations are performed on three different meshes of a plate structure using various computational strategies. Numerical results are compared to reference (analytical) solutions. It is shown that reliable results require the selection of an appropriate mesh for

resolving accurately correlation effects.

3.2 Examination of spatial correlation function

Various forms have been proposed over the years for the spatial correlation function. The particular form given by Corcos [5] is widely used. The oscillating part of the correlation function is characterized by a convected wavelength λ_c defined as :

$$\lambda_c = \frac{u_c}{f} \tag{17}$$

where $f = \omega/(2\pi)$ is the frequency (Hz).

Correlation lengths L_1, L_2 are related to the convected wavelength λ_c through :

$$L_1 = \frac{\lambda_c}{2\pi\alpha_1} \tag{18}$$

and

$$L_2 = \frac{\lambda_c}{2\pi\alpha_2} \tag{19}$$

The factor $2\pi\alpha_1$ is in the range $2\pi\,[0.10\ldots0.12] = [0.628\ldots0.754]$ while factor $2\pi\alpha_2$ is in the range $2\pi\,[0.70\ldots1.20] = [4.398\ldots7.540]$.

The correlation lengths and the convected wavelength (at 500, 1000, 2000 and 4000 Hz) are presented in Table 1 (for a flow velocity $u_c = 30\ m/s$) and in Table 2 (for a flow velocity $u_c = 150\ m/s$).

If one keeps in mind that the discretization of the oscillating part of the correlation function requires at least 8 points per wavelength (λ_c), one can conclude that the exponential decay factors (controlled by L_1 and L_2) do not introduce usually more stringent resolution requirements.

f (Hz)	L_1 (m)	L_2 (m)	λ_c (m)
500	0.0955	0.0136	0.0600
1000	0.0477	0.0068	0.0300
2000	0.0239	0.0034	0.0150
4000	0.0119	0.0017	0.0075

Table 1 – Correlation lengths L_1, L_2 and convected wavelength λ_c at various frequencies for a TBL excitation (flow velocity $u_c = 30\ m/s$, $\alpha_1 = 0.10$, $\alpha_2 = 0.70$).

f (Hz)	L_1 (m)	L_2 (m)	λ_c (m)
500	0.4775	0.0682	0.3000
1000	0.2387	0.0341	0.1500
2000	0.1194	0.0171	0.0750
4000	0.0597	0.0085	0.0375

Table 2 – Correlation lengths L_1, L_2 and convected wavelength λ_c at various frequencies for a TBL excitation (flow velocity $u_c = 150\ m/s$, $\alpha_1 = 0.10$, $\alpha_2 = 0.70$).

3.3 Element contribution to the mean quadratic pressure and the incident power spectra

The objective is to evaluate the mean quadratic pressure spectrum and the incident power spectrum using element contribution (loaded faces). This can be done by first evaluating the pressure power spectrum at an arbitrary point of the considered face. This evaluation is done hereafter for a 2-D face (4 node rectangular element) as involved in a 3-D model. The mean quadratic pressure spectrum $S_{<p^2>}$ is directly related to the incident power spectrum through :

$$S_{W_{inc}}(\omega) = \frac{1}{16\rho c} S_{<p^2>}(\omega) \tag{20}$$

On will consider the particular case of a rectangular element and evaluate the contribution of this element to the mean quadratic pressure spectrum :

$$S^e_{<p^2>}(\omega) = \frac{1}{h_1^e h_2^e} \int_{-1}^{+1} \int_{-1}^{+1} S_p(x(\xi,\eta), y(\xi,\eta), \omega)|J| d\xi d\eta \tag{21}$$

where h_1^e and h_2^e are element dimensions along x_1 and x_2 directions while $|J| = h_1^e h_2^e/4$ is the determinant of the Jacobian matrix.

The evaluation of this integral requires to set up the local pressure power spectrum $S_p(x_1, x_2, \omega)$:

$$S_p(x_1(\xi,\eta), x_2(\xi,\eta), \omega) = E\left[p(\xi,\eta,\omega)p^*(\xi,\eta,\omega)\right] \tag{22}$$

This can be done using the interpolation scheme for the sampled excitation pressure fields :

$$p(\xi,\eta,\omega) = \sum_{i=1,4} N_i(\xi,\eta) p_i(\omega) \tag{23}$$

where $N_i(\xi,\eta) = 1/4\,(1+\xi\xi_i)\,(1+\eta\eta_i)$ (with (ξ_i,η_i) = local coordinates of node i).

Substitution of equation (23) into equation (22) leads to :

$$S_p(x(\xi,\eta), y(\xi,\eta), \omega) = \sum_{i=1,4}\sum_{j=1,4} N_i(\xi,\eta) N_j(\xi,\eta) S_{p_i p_j}(\omega) \tag{24}$$

Further use of equation (24) into equation (21) leads after integration to the following result :

$$\begin{aligned} S^e_{<p^2>}(\omega) &= \frac{2}{18}\left(S_{p_1}(\omega) + S_{p_2}(\omega) + S_{p_3}(\omega) + S_{p_4}(\omega)\right) \\ &+ \frac{2}{18}\left(S_{p_1p_2}(\omega) + S_{p_2p_3}(\omega)\right) \\ &+ \frac{2}{18}\left(S_{p_3p_4}(\omega) + S_{p_1p_4}(\omega)\right) \\ &+ \frac{1}{18}\left(S_{p_1p_3}(\omega) + S_{p_2p_4}(\omega)\right) \end{aligned} \tag{25}$$

Examination of equation (25) indicates that the contribution of the considered element to the mean quadratic pressure spectrum depends not only on nodal pressure auto-power spectra but also on the cross-spectra.

If the element dimensions h_x^e and h_y^e are significant with respect to correlation lengths, $S_{p_ip_j}(\omega) << S_{ref}$ so that the following value is obtained for the mean quadratic pressure spectrum :

$$S^e_{<p^2>}(\omega) \simeq \frac{4}{9} S_{ref}(\omega) \tag{26}$$

4 Treatment of distributed random excitations

4.1 Introduction

The treatment of a diffuse field excitation in a finite element context can be organized in different ways. If the diffuse field is modeled as a weakly stationary, distributed random process, the most conventional procedure relies on the input/output relation formulated in terms of auto- and cross-PSD quantities.In a modal context, this procedure requires the evaluation of the so-called joint acceptance functions which measures the exchange of energy between the structural modes. An alternative consists in direct or algebraic sampling procedures. A direct sampling procedure relies on preliminary discretization of the diffuse field using a finite set of plane waves while the algebraic procedure is based on a simulation technique for multi-correlated fields. These techniques are reviewed in the next sections.

4.2 Conventional procedure

The usual procedure for handling a distributed random excitation in a finite element context relies on the following input/output relation :

$$S_U(\omega) = H^*(\omega) S_F(\omega) H^T(\omega) \tag{27}$$

where S_U is the PSD matrix of the nodal displacements, S_F is the PSD matrix of the nodal loads and H is the dynamic flexibility matrix (inverse of the dynamic stiffness matrix).

In the particular context of a distributed random excitation, the PSD matrix of the nodal loads can be expressed in terms of the PSD matrix S_P of the nodal pressures along the loaded surface and the coupling matrix C (allowing for the conversion of the nodal pressures into equivalent nodal loads) :

$$S_F(\omega) = C S_P(\omega) C^T \tag{28}$$

Further details can be found in [6].

4.3 Algebraic sampling procedure

A diffuse field excitation (described as a weakly stationary random process) can be sampled using the first step (generation of Fourier samples) of a simulation procedure dedicated to multi-correlated random processes ([7]).

This technique starts from a Cholesky decomposition of the positive-definite hermitian matrix S_P of order N which contains the auto- and cross-PSD of nodal pressures along the loaded surface :

$$S_P(\omega) = L(\omega) L^H(\omega) \tag{29}$$

where $L(\omega)$ is a lower triangular matrix and H denotes the complex conjugate transpose.

The procedure requires to sample phase angles ϕ_k (for $1 \leq k \leq N_e$) in the range $[0, 2\pi]$:

$$\phi_k = U(0,1)\, 2\pi \quad k = 1, \ldots, N_e \tag{30}$$

where $U(0,1)$ denotes a uniform random variable in the range $[0,1]$. A vector ς of random phase factors can be generated using these phase angles. The kth entry of this vector is given by :

$$\varsigma_k = e^{i\phi_k} \tag{31}$$

and a particular Fourier realization p^s of the distributed random process simply results from the product :

$$P^s = L(\omega)\varsigma \tag{32}$$

This particular realization supports the definition of a distributed excitation.

The generation of multiple realizations of the random processes relies on a single Cholesky decomposition of matrix S_P at each frequency. Each realization requires the selection of a particular set of phase angles and one matrix/vector product involving the vector ς of phase factors.

Each realization P^s of the random excitation leads to the evaluation of numerical response U^s (nodal displacement vector) using the deterministic input/output relation :

$$K_{dyn}(\omega) U^s(\omega) = C P^s(\omega) \quad \text{or} \quad U^s(\omega) = H(\omega) C P^s(\omega) \tag{33}$$

where H is the dynamic flexibility matrix (inverse of the dynamic stiffness K_{dyn}) while C is a coupling matrix allowing to convert sampled nodal pressures into equivalent (consistent) nodal loads.

The statistical descriptors can be produced with the usual average process. The PSD of the nodal displacement U_i is obtained as :

$$S_{U_i}(\omega) = E\left[U_i^s(\omega) U_i^{s*}(\omega)\right] \tag{34}$$

where the mathematical expectation results from the consideration of all sampled responses.

4.4 Direct sampling procedure

The direct sampling procedure for a diffuse field consists in the generation of several sets of plane waves with random phases selected according to the previous section. Each set of plane waves generates a blocked pressure excitation along the loaded boundary. Statistical operations are performed on the individual responses related to these load cases in order to evaluate S_U.

5 Application to acoustic transmission problems

5.1 Diffuse field excitation

The presented models are applied in this section to an acoustic transmission problem involving an elastic plate mounted in a rigid baffle and excited by a diffuse field. The plate is rectangular (length = 0.8 m, width = 0.6 m, thickness = 0.001 m) and is simply supported along its edges. The constitutive material is steel with conventional material properties (Young modulus $E = 2.1 \times 10^{11}$ Pa, Poisson ratio $\nu = 0.3$, loss factor $\eta = 0.02$ and mass density $\rho_s = 7850$ kg/m^3). The plate is excited by a diffuse field on one side and is radiating in a semi-infinite medium on the other side. The acoustic fluid on both sides is the air with

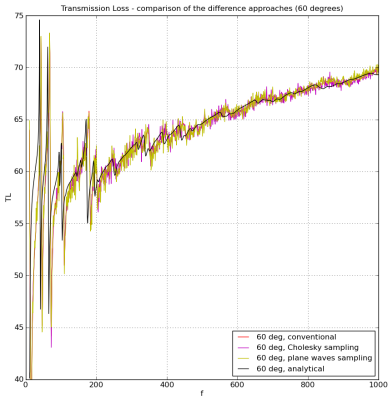

FIGURE 5 – Comparison of transmission loss obtained with different computational procedures (maximal normal incidence angle = 60 degrees).

conventional material properties (sound speed $c = 340\ m/s$ and mass density $\rho_f = 1.225\ kg/m^3$). The vibro-acoustic response is computed in the frequency band $10 - 1000$ Hz with a step of 1 Hz.

The finite element model involves 9882 nodes and 4800 shell elements. The modal description relies on the first 196 modes (eigenfrequencies below 1500 Hz). The various computational procedures available in ACTRAN software [8] are selected : treatment of the diffuse field as a weakly stationary random process using the modified spatial correlation function, generation and deterministic treatment of multiple realizations of such random process and direct sampling of the diffuse field as a sum of discrete plane waves and deterministic treatment of related realizations.

TL (transmission loss) curves computed with these procedures are compared in Figure 5 to the analytical solution for a maximum incidence angle equal to 60 degrees. All methods deliver a solution close to the reference analytical solution (based on modes up to order 15 in x and y directions).
As it can be observed, the introduction of maximum incidence angle has a small influence on global response indicators. It should be stressed however that all computations have been done with the same power spectrum for the incident pressure. The influence of the silent cone on the incident pressure is therefore not considered in this study which focuses only on the effect of the modified correlation function.

5.2 Turbulent boundary layer excitation

An acoustic transmission problem is selected for studying the effect of the mesh resolution on the treatment of a TBL excitation. The considered problem involves a rectangular plate (size along $x_1 = 0.47\ m$, size along $x_2 = 0.37\ m$, thickness $= 0.005\ m$). The constitutive material is steel (Young modulus $E = 2.0\ 10^{10}\ Pa$, loss factor $\eta = 0.02$; Poisson ratio $\nu = 0.3$, density $\rho_s = 7800\ kg/m^3$). The plate is simply supported along its edges. The plate is excited by a TBL on one side and is radiating in a semi-infinite medium on the other side. The following characteristics are selected for the TBL excitation : $S_{ref} = 1\ Pa^2/Hz$, $\alpha_1 = 0.10$ (−), $\alpha_2 = 0.70$ (−) while the following flow velocity values are considered : 10 and 100 m/s. The analysis is performed in the frequency band [10, 1000] Hz using different computational strategies : (1) physical approach with conventional solution procedure, (2) modal approach with conventional solution procedure and (3) modal approach with sampling procedure.

5.2.1 Selected FE meshes

Three meshes are selected for the FE analysis (and for sampling the TBL excitation). Mesh M1 : 24×19 subdivisions (element size $\simeq 0.020$ m), Mesh M2 : 32×25 subdivisions (element size $\simeq 0.015$ m) and Mesh M3 : 47×37 subdivisions (element size $= 0.010$ m). Mesh resolutions are indicated in Table 3 for the different flow velocities.

u_c (m/s)	λ_c (m)	λ_c/h (M1) (-)	λ_c/h (M2) (-)	λ_c/h (M3) (-)
10	0.010	1/2	2/3	1
100	0.100	5	20/3	10

TABLE 3 – Resolution (λ_c/h where $\lambda_c = u_c/f$ is the convected wavelength and h the element size) of meshes M1, M2 and M3 wrt. TBL excitation at 1000 Hz for different flow velocities ($u_c = 10, 100$ m/s).

5.2.2 Evaluation of radiated power

For illustration purposes, the radiated power computed with a FE model based on mesh M1 is represented at Figures 6 and 7 for two representative flow velocities. Numerical results obtained with physical/conventional, modal/conventional and modal/sampled (50 realizations) approaches are compared to the exact solution.

Observation of these figures (and results related to other flow velocities and FE meshes) show that considered meshes are not able to capture the exact solution for low flow velocities (10 m/s). This is due to a too coarse mesh for resolving the TBL excitation.

5.2.3 Evaluation of incident power

The pseudo incident power related to a TBL excitation results form the integration of the pseudo incident intensity $S_{\langle p^2 \rangle}/(16\rho c)$ along the loaded surface. The exact result is therefore $0.26095\ 10^{-4}\ W$. The approximate result is obtained by integrating the local pressure auto-spectrum (divided by the factor $16\rho c$) along individual elements. The related results for the considered flow velocities are compared to the exact result in Figure 8 (for mesh M1).

Further examination of these figures indicate that a sufficient mesh resolution is requested for capturing correctly the incident power, especially at low flow velocities and at high frequencies.

In contrast, the evaluation of the incident power for a diffuse field along the same meshes for the same frequency band is leading to approximate values closed to the exact result.

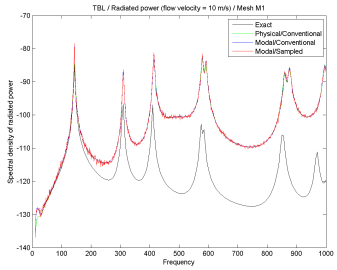

FIGURE 6 – Power radiated by a plate excited by a TBL (u_c= 10 m/s, $\alpha_1 = 0.10$, $\alpha_2 = 0.70$) : comparison of exact and approximate solutions physical/conventional, modal/conventional and modal/sampled (50 realizations) approaches with mesh M1.

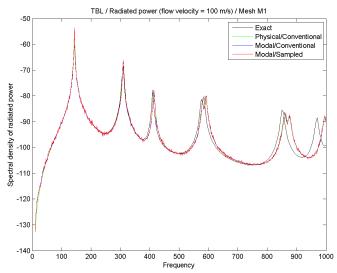

FIGURE 7 – Power radiated by a plate excited by a TBL (u_c = 100 m/s, $\alpha_1 = 0.10$, $\alpha_2 = 0.70$) : comparison of exact and approximate solutions using physical/conventional, modal/conventional and modal/sampled (50 realizations) approaches with mesh M1.

5.2.4 Evaluation of transmission loss

The transmission loss can be evaluated using the exact value of the incident power or the approximate value resulting form the integration of the mean quadratic pressure indicator along the loaded surface. This is illustrated (for mesh M1) in Figure 9 ($u_c = 10\ m/s$).

Examination of this figure shows that the insufficient mesh resolution for capturing correctly correlation effects within the TBL doest not allow for an accurate evaluation of the transmission loss. The discretized form of the incident power (instead of the exact one) do not introduce a compensation effect so the the related TL value can be worst.

6 Conclusion

Some particular aspects related to the handling of distributed random excitations (diffuse field and turbulent boundary layer) have been addressed. Elimination of grazing incidences for a diffuse field has been performed in order to extract a modified spatial correlation function. Mesh resolution issues related to turbulent boundary layer excitations have been highlighted.

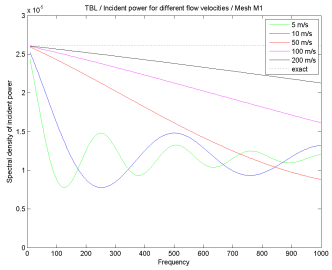

FIGURE 8 – Comparison of exact and approximate pseudo-incident powers related to a TBL excitation as computed by integration along mesh M1 (u_c = 5 – 200 m/s, $\alpha_1 = 0.10$, $\alpha_2 = 0.70$).

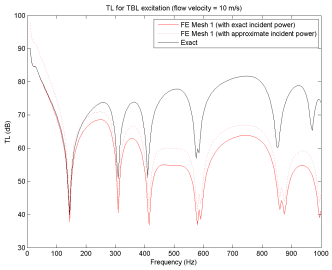

FIGURE 9 – Comparison of TL indicators for TBL excitation along mesh M1 (u_c = 10 m/s, $\alpha_1 = 0.10$, $\alpha_2 = 0.70$).

Références

[1] Jacobsen F. The diffuse sound field. Technical report, Technical University of Denmark, Acoustic Laboratory, Report N 27, 1979.

[2] Chun I., Rafaely B., and Joseph P. Experimental investigation of spatial correlation in broadband reverberant sound fields. *Journal of the Acoustical Society of America*, 113 :1995–1998, 2003.

[3] Rafaely B. Spatial-temporal correlation of a diffuse sound field. *Journal of the Acoustical Society of America*, 107 :3254–3258, 2000.

[4] Van Den Nieuwenhof B., Lielens G., and Coyette J.P. An enhanced modal approach for random vibro-acoustics. In *ISMA Conference, Leuven*. KUL, September 2008.

[5] Corcos G.M. Resolution of pressure in turbulence. *Journal of the Acoustical Society of America*, 35 :192–199, 1963.

[6] Coyette J.P. and Meerbergen K. An efficient computational procedure for random vibro-acoustic simulations. *Journal of Sound and Vibration*, 310 :448–458, 2008.

[7] Wittig L.E. and Sinha A.K. Simulation of multi-correlated random processes using the FFT algorithm. *Journal of the Acoustical Society of America*, 58 :630–634, 1975.

[8] Actran 14 user's manual. Technical report, Free Field Technologies, 2013.